Available online at www.sciencedirect.com

ScienceDirect

Nuclear Physics A 952 (2016) 100–120

NUCLEAR PHYSICS A

www.elsevier.com/locate/nuclphysa

Measurement of fission products yields in the quasi-mono-energetic neutron-induced fission of ^{232}Th

H. Naik [a,*], Sadhana Mukherji [b], S.V. Suryanarayana [c], K.C. Jagadeesan [d], S.V. Thakare [d], S.C. Sharma [c]

[a] *Radiochemistry Division, Bhabha Atomic Research Centre, Mumbai - 400 085, India*
[b] *Reactor Physics Design Division, Bhabha Atomic Research Centre, Mumbai- 400 085, India*
[c] *Nuclear Physics Division, Bhabha Atomic Research Centre, Mumbai - 400 085, India*
[d] *Radiopharmaceutical Division, Bhabha Atomic Research Centre, Mumbai - 400 085, India*

Received 14 December 2015; received in revised form 18 February 2016; accepted 4 April 2016

Available online 14 April 2016

Abstract

The cumulative yields of various fission products in the ^{232}Th(n, f) reaction at average neutron energies of 5.42, 7.75, 9.35 and 12.53 MeV have been determined by using an off-line γ-ray spectrometric technique. The neutron beam was produced from the ^{7}Li(p, n) reaction by using the proton energies of 7.8, 12, 16 and 20 MeV. The mass chain yields were obtained from the cumulative fission yields by using the charge distribution correction of medium energy fission. The fine structure in the mass yield distribution was interpreted from the point of nuclear structure effect. On the other hand, the higher yield around mass number 133–134 and 143–144 as well as their complementary products were explained based on the standard I and standard II asymmetric mode of fission. From the mass yield data, the average value of light mass ($\langle A_L \rangle$), heavy mass ($\langle A_H \rangle$), the average number of neutrons ($\langle \nu \rangle$) and the peak-to-valley (P/V) ratios at different neutron energies of present work and literature data were obtained in the ^{232}Th(n, f) reaction. The different parameters of the mass yield distribution in the ^{232}Th(n, f) reaction were compared with the similar data in the ^{232}Th(γ, f) reaction at comparable excitation energy and a **surprising** difference was observed.

Keywords: Nuclear reactions; ^{232}Th(n, F); $E_n = 5.42$; 7.75, 9.35 and 12.53 MeV; Off-line γ-ray spectrometric technique; measured fission product yields; mass yield distributions

* Corresponding author.
E-mail address: naikhbarc@yahoo.com (H. Naik).

http://dx.doi.org/10.1016/j.nuclphysa.2016.04.003
0375-9474/

1. Introduction

In recent times, major effort of the nuclear scientist is to generate nuclear-power based on the concept of fast reactors [1–5], advanced heavy-water reactors (AHWR) [6,7] and accelerator-driven sub-critical systems (ADSs) [8–13] to fulfill the increased demand for power production. In AHWR, ^{232}Th–^{233}U is the primary fuel for power generation. On the other hand, ^{232}Th–^{233}U fuel in connection with ADSs [8–13] is one of the possibilities for power generation besides transmutation of long-lived fission products (e.g., ^{93}Zr, ^{99}Tc, ^{107}Pd, ^{129}I, ^{135}Cs) and incineration of long-lived minor actinides (e.g., ^{237}Np, ^{240}Pu, ^{241}Am, ^{243}Am, ^{244}Cm) to solve the problem of radioactive waste, which generates from the conventional nuclear reactors. Thus, the concept of the energy amplifier (EA) [8–13] in the hybrid system is based on the thorium fuel cycle and a spallation neutron source in ADSs. The ^{232}Th–^{233}U fuel in AHWR and ADSs has an advantage over the present reactor based on uranium fuel from the point of production of thousand times less radiotoxic waste (long-lived minor actinides) in the former than the latter [14]. Besides these, thorium in the Earth's crust is three to four times more abundant than uranium [14]. Thus, it is a fact that ^{232}Th is the only nucleus present in nature, which can give rise to an excess of fissile material ^{233}U in presence of either thermal or fast neutrons, and thus making it an excellent choice for nuclear reactors of the future. In the thorium-uranium fuel cycle, the fissile nucleus ^{233}U is generated by two successive β-decays after a neutron capture by the fertile nucleus ^{232}Th.

In ADSs the high energy (GeV) proton from an accelerator strikes a heavy element like Pb or Bi, which yields a large number of neutrons by spallation reaction. The spallation target becomes a source of neutrons, which drives a self-sustaining fission chain in a sub-critical core. In the spallation processes, along with high-energy neutrons, high-energy photons are also produced. The high-energy neutrons and photons cause fission and different types of nuclear reactions of the long-lived minor actinides, spallation target and the ^{232}Th of the hybrid systems. In the fission process numbers of fission products are produced. The yields of fission products are needed for decay heat calculations [15], which are necessary for the design of ADSs. Thus it is important to study the distribution fission products yields i.e. mass yield distribution [16–18] in the high energy neutron and photon induced fission of Pb, Bi, Th and long-lived minor actinides. Mass yield distribution studies in the low energy neutron and photon induced fission of actinides provide important information about the effect of nuclear structure besides dynamics of descent from saddle to scission point [16,17]. It is a well-known fact that the mass yield distributions [16,17] in the neutron and photon induced fission of pre-actinides (e.g. Pb, Bi) and heavy-Z actinides (e.g. Es to Lr) are symmetric in nature, whereas for medium-Z actinides (e.g. U to Cf), are asymmetric in nature. On the other hand, the mass yield distributions in the neutron and photon induced fission of light-Z actinides (e.g. Ac, Th, Pa) are asymmetric with triple humped [16,17]. However, with increase of excitation energy and Z of the actinides, mass yield distribution changes from asymmetric to symmetric and the effect of nuclear structure decreases. In the neutron induced fission, the compound nucleus has one neutron more than the target, whereas in the photon induced fission, the compound nucleus is the target with excited state.

Sufficient data on fission product yields relevant to mass yield distribution in the neutron-induced fission of ^{232}Th are available in different compilations [18–23]. On the other hand, the mass yields of fission products in the photon (bremsstrahlung) induced fission of ^{232}Th are available only in the EXFOR compilation [23]. From the EXFOR compilation, it can be seen that sufficient data on fission product yields are available in the reactor neutron [24,25] as well as in the 2–8 and 14 MeV mono-energetic neutron [26–48] induced fission of ^{232}Th. Yields of fission products in the 6.35, 8.53 and 10.09 MeV quasi-mono-energetic neutron fission of ^{232}Th are de-

termined by us [49,50] by using the off-line gamma ray spectrometric technique. Similarly, mass yield distribution in the 33–60 MeV quasi-mono-energetic neutron fission of ^{232}Th is determined by Ryzhov et al. [51] by using the physical measurement. On the other hand, the yields of fission products in the bremsstrahlung induced fission of ^{232}Th at the end-point energies of 6 MeV to 3 GeV are available in literature [52–62]. Similarly, the fission fragment yields data of neutron-deficient Th isotopes such as $^{220-229}$Th in the excitation energy range of the GDR region due to electromagnetic fission in inverse kinematics are available in Refs. [63–65]. From these data, it was observed that the yields of fission products are available in a wide range of neutron- [24–51] and bremsstrahlung- [52–62] induced fissions of ^{232}Th. However, the fission product yields data within neutron energies of 8 to 14.8 MeV are available in limited way except our data at the neutron energies of 6.35, 8.53 and 10.09 MeV [50].

From the above experimental data, it can be seen that in both the neutron [24–51] and bremsstrahlung [52–65] induced fission of ^{232}Th, the yields of fission products are higher around mass numbers (A) 133–135, 138–140 and 143–145 and their complementary products due to nuclear structure effect [50,60–62]. However, the yields of fission products for $A = 133$–135 are more pronounced in the ^{232}Th(n, f) reaction [24–51] than in the ^{232}Th(γ, f) reaction [52–65]. From the above data, it is not clear at what neutron and bremsstrahlung energy the nuclear structure disappears. Further from the existing literature data, it can be seen that the mass yield distribution in both the neutron [24–51] and bremsstrahlung [52–65] induced fission of ^{232}Th are asymmetric with triple humped. It is also observed that the peak-to-valley (P/V) ratio decreases with increase of excitation energy. However, the decrease of peak-to-valley ratio with the increase of excitation energy in neutron- and bremsstrahlung induced fission of ^{232}Th are not similar. So far a systematic study on this observation has not been made due to the unavailability of mass yield data in a wide range of neutron energies [24–51] unlike in the bremsstrahlung energies [52–65]. In view of the above facts, in the present work the yields of various fission products in the ^{232}Th(n, f) reaction with average neutron energies of 5.42, 7.75, 9.35 and 12.53 MeV have been determined by using an off-line γ-ray spectrometric technique. From the yields of the fission products, their mass yields were obtained by using the charge distribution correction [18,66]. The fission product yields data at different neutron energies of the present work and the literature data in the ^{232}Th(n, f) reaction [26–50] are compared with the similar data in the ^{232}Th(γ, f) reaction [52–62] to examine the role of excitation energy on the nuclear structure effect. The variation of peak-to-valley (P/V) ratio, average light ($\langle A_L \rangle$) and heavy ($\langle A_H \rangle$) masses as well the average neutron number ($\langle \nu \rangle$) as a function of excitation energy have also been discussed.

2. Experimental details

In the present experiment, the proton beam from the 14UD BARC-TIFR Pelletron facility at Mumbai, India [49,50] was used to produce the quasi-mono-energetic neutron beam based on the ^{7}Li$(p, n)^{7}$Be reaction. The natural lithium metal foil with thickness of 3.7 mg/cm^2 was used, which was sandwiched between two tantalum foils of different thickness. The front tantalum foil facing the proton beam is 3.9 mg/cm^2 thick, in which degradation of proton energy is only 50–80 keV [67]. On the other hand the back tantalum foil is 0.025–0.1 mm thick, which is sufficient to stop the proton beam. A collimator of 6 mm diameter was used before the Li target to avoid the energy spread of the proton beam. Behind the Ta–Li–Ta stack, the ^{232}Th metal foil wrapped with 0.025 mm thick super pure aluminum foil was used for irradiation. The aluminum wrapper was used as a catcher foil to stop fission products recoiling out from the ^{232}Th metal foil during the irradiation. The size of each ^{232}Th metal foil was 1.0 cm^2 with thickness of about

323.7–325.2 mg/cm^2. The Al wrapped ^{232}Th sample was mounted at zero degree angle in the forward direction with respect to the beam direction at a distance of 2.1 cm from the location of the Ta–Li–Ta stack. Four different sets of Ta–Li–Ta stacks and Al wrapped ^{232}Th samples were made for irradiations with four different neutron energies. The neutrons beam was generated by impinging the proton beam on the lithium metal foil through the thin tantalum foil of the Ta–Li–Ta metal stack.

The Al wrapped ^{232}Th sample was irradiated for 4–15 h depending upon the proton energy faced by the front tantalum foil. The proton energies used in the present work were 7.8, 12, 16 and 20 MeV, respectively. The proton current during the irradiations varied within 200 to 400 nA. The corresponding maximum energies of the neutron beam impinging on the ^{232}Th samples were 5.92, 10.12, 14.12 and 18.12 MeV, respectively. After each irradiation, the samples were cooled for 1–2 h. Then the irradiated ^{232}Th targets along with Al catcher were mounted on different Perspex plates. The γ-rays counting of the fission products from the irradiated samples were done in energy and efficiency calibrated 80 cm^3 HPGe detector coupled to a PC-based 4 K channel analyzer. The dead time of counting was always kept less than 5% by placing the irradiated sample at a suitable distance from the end cap of the detector to avoid pileup effects. The γ-ray counting of the sample was done in live time mode and was followed as a function of time. The resolution of the detector system during counting was 1.8 keV FWHM at 1332.5 keV of ^{60}Co. The energy and efficiency calibration of the detector system was performed by using the 121.8 to 1408.01 keV γ-rays of a standard ^{152}Eu source at same geometry, where the summation error was negligible. This was checked by comparing the efficiency obtained from γ-ray counting of standards such as ^{241}Am (59.5 keV), ^{133}Ba (80.9, 276.4, 302.9, 356.0 and 383.8 keV), ^{137}Cs (661.7 keV), ^{54}Mn (834.6 keV), ^{60}Co (1173.2 and 1332.5 keV). The detector efficiency was 20% at 1332.5 keV, relative to 3″ diameter x3″ length NaI(Tl) detector. The uncertainty in the efficiency was 2–3%. For each irradiated samples, several sets of measurements were done with increasing counting time to have a good counting statistics for different fission products with the half-life ranging from 52.5 minutes to 64.02 days. The γ-ray counting of the irradiated ^{232}Th samples was done up to few months to check the half-life of the fission products of interest.

3. Calculation and results

3.1. Calculation of the neutron energy

In the present experiment, the quasi-mono-energetic neutron beam were produced from the ^{7}Li(p, n) reaction [68–70] of the natural lithium. The isotopic abundances of ^{6}Li and ^{7}Li in natural lithium are 7.59% and 92.41%, respectively. Different reactions of proton with natural lithium are as follows:

No.	Reaction	Q-value (MeV)	Threshold energy (MeV)
1.	^{6}Li(p, n)^{6}Be	−5.07	5.92
2.	^{6}Li(p, np)^{5}Be	−5.67	6.62
3.	^{7}Li(p, n)^{7}Be (ground-state transition)	−1.644	1.881
4.	^{7}Li(p, n)^{7}Be* (first excited-state transition)	−2.079	2.38
5.	^{7}Li(p, n^3He)^{4}He (three-body break up reaction)	−3.23	3.6
6.	^{7}Li(p, n)^{7}Be**	−6.18	7.06

Among these, the reactions 3, 4 and 5 primarily contribute to the number of neutrons, while reactions 1, 2 and 6 do not contribute significantly. It can be seen from the above table that the

Q-value for the ^{7}Li(p, n)^{7}Be reaction to the ground state transition is -1.644 MeV, whereas the first excited state is 0.431 MeV above ground state leading to an average Q-value of -1.868 MeV. However, the threshold value to populate the ground state of ^{7}Be is 1.881 MeV. Thus, for the proton energies of 7.8, 12, 16 and 20 MeV, the resulting peak energies of first group of neutrons (n_0) will be 5.92, 10.12, 14.12 and 18.12 MeV, respectively. Above the proton energy of 2.37 MeV, the n_1 group of neutron is also produced. Thus the corresponding neutron energies of second group of neutrons (n_1), for the first excited state of ^{7}Be will be 5.43, 9.63, 13.63 and 17.63 MeV, respectively. The branching ratio to the ground state and first excited state of ^{7}Be up to $E_p = 7$ MeV is given by Liskien and Paulsen [68]. Similarly, Meadows and Smith [69] have also given the branching ratio to the ground state and first excited state of ^{7}Be up to 7 MeV. On the other hand, Poppe et al. [70] have given the branching ratio to the ground state and first excited state of ^{7}Be for $E_p = 4.2$ MeV to 26 MeV. Above proton energy of 4.5 MeV, the fragmentation of ^{8}Be to ^{4}He + ^{3}He + n ($Q = -3.23$ MeV) takes place, which causes continuous neutron energy distribution besides the n_0 and n_1 groups of neutrons. Meadows and Smith [69] have given experimental neutron distributions from the break up channels and also parameterized these distributions. We have generated the neutron spectra using the neutron energy distribution given by C.H. Poppe et al. [70] and shown in our earlier work [49,50]. From the neutron spectra, the flux-weighted average neutron energies were calculated as 5.42, 7.75, 9.35 and 12.53 MeV, respectively. The energy spread for the above average neutron energies are around 0.3 to 0.7 MeV [49,50].

3.2. Calculation of fission product yields from the photo-peak areas

From the total peak areas, the numbers of detected γ-rays (N_{obs}) for the fission products of interest were obtained by subtracting the linear Compton background. From N_{obs} of an individual fission product, the cumulative yields (Y_R) relative to ^{92}Sr were calculated by using the usual decay equation [50],

$$Y_R = \frac{N_{obs}(CL/LT)\lambda}{n\sigma_f\varphi I_\gamma \varepsilon(1-e^{-\lambda t})e^{-\lambda T}(1-e^{-\lambda CL})} \tag{1}$$

where n is the number of target atoms, φ is the neutron flux and σ_f is the neutron fluxed average fission cross section of ^{232}Th at 5.42, 7.75, 9.35 and 12.53 MeV. I_γ is the γ-ray intensity or γ-ray emission probability, ε is the detection efficiency of the γ rays in the detector system and λ is the decay constant of the fission-product of interest ($\lambda = \ln 2/T_{1/2}$). t and T are the irradiation and cooling times, whereas, CL and LT are the real time and the live time of counting, respectively. The nuclear spectroscopic data, such as the γ-ray energies, the half-lives ($T_{1/2}$), and the γ-ray intensity (I_γ) of the fission products were taken from the literature [71,72].

The $n\sigma_f\varphi$ term in Eq. (1) was first obtained from the photo-peak activity of 1383.9 keV γ-line and by assuming the cumulative yield (Y_R) of ^{92}Sr as 1.0. Thus the individual terms such as n, σ_f and φ are not necessary to be used separately. The $n\sigma_f\varphi$ term and the photo-peak activities of the γ-lines of other fission products were then used in Eq. (1) to obtain their relative cumulative yields (Y_R). For some of the fission product like ^{112}Ag, its precursor ^{112}Pd is long-lived ($T_{1/2} = 21.03$ h). Thus there is equilibrium between ^{112}Pd and ^{112}Ag. The cumulative yield of ^{112}Pd and independent yield of ^{112}Ag is possible to obtain from decay-growth equation by using the activity of the 617.5 keV γ-line. Otherwise the half-life of ^{112}Pd and the activity of 617.5 keV γ-line can be used to determine the cumulative yield of ^{112}Ag, which has been done in the present work. Similar is the problem for the fission products ^{105}Ru–^{105}Rh, ^{131}Sb–^{131}I,

^{134}Te–^{134}I, ^{141}Ba–^{141}Ce and ^{142}Ba–^{142}La. As for example, in the case of ^{134}Te–^{134}I, it is necessary to use the decay-growth equation and the activity of the 847.3 and 884.1 keV γ-lines to determine the cumulative yield of ^{134}Te and independent yield of ^{134}I. Otherwise it is necessary to wait up to the six half-lives decay of ^{134}Te and then the equation (1) can be used to determine the cumulative yield of ^{134}I from the activities of 847.3 and 884.1 keV γ-lines. In the present work, the later method was followed to determine the cumulative yield of ^{134}I. Similar is the case for the cumulative yields of the fission products ^{105}Rh, ^{131}I, ^{141}Ce and ^{142}La, respectively. From the Y_R values of the fission products, their relative mass yields (Y_{RA}) were calculated after correcting for charge distribution [18,66]. According to Wahl's prescription [18], the fractional cumulative yield (Y_{FCY}) of a fission product in an isobaric mass chain is given as

$$Y_{FCY} = \frac{EOF^{a(Z)}}{\sqrt{2\pi\sigma^2}} \int_{-\infty}^{Z+0.5} \exp\left[-(Z - Z_P)^2/2\sigma 2\right] dZ \tag{2}$$

$$Y_{RA} = Y_R / Y_{FCY} \tag{3}$$

Where Z_P is the most probable charge and σ_z is the width parameter of an isobaric-yield distribution. $EOF^{a(Z)}$ is the even–odd effect with $a(Z) = +1$ for even-Z nuclides and -1 for odd-Z nuclides.

It can be seen from the Eq. (2) and (3) that in an isobaric mass chain, it is necessary to have knowledge of Z_P, σ_z and $EOF^{a(Z)}$ to calculate the Y_{FCY} value of a fission product and thus the relative mass yield (Y_{RA}). The $EOF^{a(Z)}$ values in the medium energy fission is negligible. On the other hand, the σ_z value in medium energy fission of actinide is 0.70 ± 0.06 [66]. This value is based on the data of medium energy proton and alpha induced fission of ^{232}Th and ^{238}U as shown by Umezawa et al. [66]. The Z_P values of individual mass chain (A) in the neutron induced fission of ^{232}Th at the average energies of 5.42, 7.75, 9.35 and 12.53 MeV were also calculated based the prescription of Umezawa et al. [66] as

$$Z_P = \eta Z_F \pm \Delta Z_P, \qquad \eta Z_F = Z_{UCD} = (Z_F/A_F)(A + \nu_{post}) \tag{4a}$$

$$\eta = (A + \upsilon_{post})/(A_C - \upsilon_{pre}), \qquad A_F = A_C - \nu_{pre} \tag{4b}$$

where Z_C and A_C are the charge and mass of the compound nucleus. Z_F and A_F are the charge and mass of the fissioning system (^{233}Th*). ν_{pre} and ν_{post} are pre- and post-fission neutrons at scission. Z_{UCD} is the most probable charge based on the unchanged charge-density distribution as suggested by Sugarman and Turkevich [73]. A is the mass of the fission product and ΔZ_P ($= Z_P - Z_{UCD}$) is the charge-polarization parameter. The $+$ and $-$ signs for the ΔZ_P value are applicable to light and heavy fragments, respectively.

The pre- (ν_{pre}) and post-scission (ν_{post}) neutrons in medium-energy fission of actinides can be calculated using the formula of Umezawa et al. [66] or Strecker et al. [74]. The saw tooth nature of post-fission neutron emission as a function of the fission fragment mass is possible to obtain by Strecker et al. [74]. In the present work we have used the prescription of Umezawa et al. [66] because the other parameters describing the charge distribution systematic were also taken from Ref. [66]. Accordingly, the pre- (ν_{pre}) and post-scission (ν_{post}) neutrons were calculated from the excitation energy (E^*) of the compound nucleus using the following relations [66].

$$\nu_{pre} = \frac{E^*}{7.5 \pm 0.5} + \frac{Z_C}{2A_C} - (19.0 \pm 0.5) \tag{5a}$$

$$\nu_{post} = \begin{cases} 1.0 & \text{for } A > 88 \\ 1.0 + 0.1(A - 88) & \text{for } 78 < A < 88 \\ 0 & \text{for } A < 78 \end{cases} \quad (5b)$$

In the 5.42, 7.75, 9.35 and 12.53 MeV neutron induced fission of ^{232}Th, the excitation energy (E*) of the compound nucleus (^{233}Th*) are 10.03, 12.16, 14.96 and 17.14 MeV, respectively. The E* values were used in Eq. (5a) to calculate the ν_{pre} values for four different neutron energies, whereas the ν_{post} as a function of mass number were determined by using Eq. (5b). The ν_{pre} and ν_{post} values obtained from Eqs. (5a) and (5b) were used in Eqs. (4a) and (4b) to calculate the value of Z_{UCD} as a function of mass number for the different fission products. The ΔZ_P value was then calculated from the following relation [66]:

$$\Delta Z_P = 0 \quad \text{for } I\eta - 0.5I < 0.04 \quad (6a)$$

$$\Delta Z_P = (20/3)(I\eta - 0.5I - 0.04) \quad \text{for } 0.04 < I\eta - 0.5I < 0.085 \quad (6b)$$

The Z_P value as a function of mass number and the average width parameter (σ_z) of 0.7 from Ref. [66] were used in Eq. (2) to obtain the Y_{FCY} values for individual fission products. The relative mass yield (Y_{RA}) of the fission products from their relative cumulative yield (Y_R) were obtained in Eq. (3) by using the Y_{FCY} values of different fission products. The relative mass yields (Y_{RA}) of the fission products obtained were then normalized to a total yield of 200% to calculate the absolute mass yields (Y_A). The absolute cumulative yields (Y_C) of the fission products in the 5.42, 7.75, 9.35 and 12.53-MeV neutron-induced fission of ^{232}Th were then obtained from the mass yield data and Y_{FCY} values by using the Eq. (7), which is the modified form of Eq. (3).

$$Y_C = Y_A \times Y_{FCY} \quad (7)$$

The absolute cumulative yield (Y_C) and mass yield (Y_A) of the fission products in the 5.42, 7.75, 9.35 and 12.53-MeV neutron-induced fission of ^{232}Th along with the nuclear spectroscopic data from Refs. [71,72] are given in Tables 1–4, respectively. The uncertainty shown in the measured cumulative yield of the individual fission products shown in Tables 1–4 is the statistical fluctuation of the mean value from replicate measurements. The overall uncertainty is the contributions from both random and systematic errors. The random error in the observed activity is due to counting statistics and is estimated to be 5–10%, which can be determined by accumulating the data for the optimum period of time, depending on the half-life of the nuclide of interest. On the other hand, the systematic errors are due to the uncertainties in the irradiation time (0.1%), detector efficiency calibration (~3%), half-life of nuclides of the fission products (~1%) and the γ-ray abundance or branching intensity (~2%), which are the largest variation in the literature [71,72]. The branching intensity used for each decay chain varies, which is shown in the Ref. [71]. Thus, the overall systematic error is about 3.7%. An upper limit of error of 6.2–10.7% was determined for the fission product yields based on the random error of 5–10% and a systematic error of 3.7%.

4. Discussion

The yields of fission products in the ^{232}Th(n, f) reaction at average neutron energies of 5.42, 7.75, 9.35 and 12.53 MeV shown in Tables 1–4 are determined for the first time. The mass yield data in the ^{232}Th(n, f) reaction from the present work for the above four average neutron

Table 1
Nuclear spectroscopic data and yields of fission products in the 5.42 MeV neutron-induced fission of ^{232}Th.

Nuclide	Half-life	γ-Ray energy (keV)	γ-Ray abundance (%)	Y_C (%)	Y_A (%)
^{85}Kr^{m}	4.48 h	151.2	75.0	3.832 ± 0.346	3.832 ± 0.346
		304.9	14.0	3.918 ± 0.101	3.846 ± 0.101
^{87}Kr	76.3 min	402.6	49.6	5.859 ± 0.572	5.877 ± 0.574
^{88}Kr	2.84 h	196.3	25.9	5.778 ± 0.415	5.872 ± 0.422
^{91}Sr	9.63 h	749.8	23.6	5.782 ± 0.427	5.782 ± 0.427
		1024.3	33.0	6.223 ± 0.683	6.223 ± 0.683
^{92}Sr	2.71 h	1383.9	90.0	5.453 ± 0.052	5.464 ± 0.052
^{93}Y	10.18 h	266.9	7.3	5.369 ± 0.555	5.369 ± 0.555
^{95}Zr	64.02 d	724.3	44.2	6.664 ± 0.678	6.664 ± 0.678
^{97}Zr	16.91 h	743.4	93.0	4.639 ± 0.422	4.643 ± 0.422
^{99}Mo	65.94 h	140.5	89.4	2.874 ± 0.228	2.874 ± 0.228
		739.5	12.13	3.107 ± 0.247	3.107 ± 0.247
^{103}Ru	39.26 d	497.1	90.0	0.479 ± 0.128	0.479 ± 0.128
^{105}Rh	35.36 h	319.1	19.2	0.128 ± 0.014	0.128 ± 0.014
^{112}Ag	3.13 h	617.5	43.0	0.204 ± 0.033	0.204 ± 0.033
^{115}Cd^{g}	53.46 h	527.9	27.45	0.180 ± 0.033	
^{115}Cd^{total}				0.209 ± 0.038*	0.209 ± 0.038*
^{127}Sb	3.85 d	687.0	37.0	0.498 ± 0.081	0.498 ± 0.081
^{128}Sn	59.07 min	482.3	59.0	0.993 ± 0.107	1.058 ± 0.114
^{129}Sb	4.32 h	812.4	43.0	1.631 ± 0.146	1.641 ± 0.147
^{131}I	8.02 d	364.5	81.7	3.007 ± 0.242	3.007 ± 0.242
^{132}Te	3.2 d	228.1	88.0	3.604 ± 0.287	3.633 ± 0.289
^{133}I	20.8 h	529.9	87.0	4.796 ± 0.606	4.811 ± 0.607
^{134}I	52.5 min	847.3	95.9	6.835 ± 0.615	6.849 ± 0.617
		884.09	65.0	6.750 ± 0.521	6.764 ± 0.522
^{135}I	6.57 h	1131.5	22.7	5.746 ± 0.352	5.810 ± 0.356
		1260.4	20.3	5.817 ± 0.464	5.881 ± 0.470
^{139}Ba	83.03 min	165.8	23.7	7.565 ± 0.455	7.565 ± 0.455
^{140}Ba	12.75 d	537.3	35.4	8.177 ± 0.574	8.177 ± 0.574
^{141}Ce	32.5 d	145.4	20.5	7.314 ± 0.493	7.314 ± 0.493
^{142}La	91.1 min	641.3	47.0	6.137 ± 0.394	6.137 ± 0.394
^{143}Ce	33.03 h	293.3	42.8	6.432 ± 0.361	6.432 ± 0.361
^{147}Nd	10.98 d	531.0	13.1	2.275 ± 0.161	2.281 ± 0.161
^{150}Pm	2.68 h	333.97	68.0	0.522 ± 0.047	0.522 ± 0.047

Y_C – Cumulative yields, Y_A – Mass yields, ^{92}Sr – Fission rate monitor.
* The yields of ^{115}Cd^{total} is based on the ratio of ^{115}Cd^{g}/^{115}Cd^{m} = 6 as done in Ref. [50].

energies are plotted in Fig. 1 as a function of their mass number. The neutron induced fission of ^{232}Th at 5.42, 7.75, 9.35 and 12.53 MeV correspond to the average excitation energies of 10.03, 12.36, 13.96 and 17.14 MeV respectively. The 16, 25, 35 and 45 MeV bremsstrahlung induced fission of ^{232}Th correspond to the comparable average excitation energies of 11.12, 13.22, 14.7 and 16.95 MeV, respectively. Thus the fission products yields for ^{232}Th(γ, f) with the bremsstrahlung end-point energies of 16, 25, 35 and 45 MeV from literature [55,60,62] are plotted in Fig. 2 for comparison. It can be seen from Fig. 1 and Fig. 2 that for comparable excitation energies, the mass yield distribution for both the ^{232}Th(n, f) and ^{232}Th(γ, f) reactions are triple humped as in the case of electromagnetic fission in inverse kinematics for neutron-deficient $^{220-229}$Th isotopes [63–65]. It can be seen from Fig. 1 and Fig. 2 that in both the neutron

Table 2
Nuclear spectroscopic data and yields of fission products in the 7.75 MeV neutron-induced fission of ^{232}Th.

Nuclide	Half-life	γ-Ray energy (keV)	γ-Ray abundance (%)	Y_C (%)	Y_A (%)
^{85}Kr^{m}	4.48 h	151.2	75.0	3.331 ± 0.137	3.331 ± 0.137
		304.9	14.0	3.827 ± 0.217	3.827 ± 0.217
^{87}Kr	76.3 min	402.6	49.6	5.677 ± 0.170	5.694 ± 0.170
^{88}Kr	2.84 h	196.3	25.9	5.551 ± 0.112	5.642 ± 0.113
^{91}Sr	9.63 h	749.8	23.6	5.783 ± 0.406	5.783 ± 0.406
		1024.3	33.0	6.005 ± 0.567	6.005 ± 0.567
^{92}Sr	2.71 h	1383.9	90.0	5.201 ± 0.052	5.212 ± 0.052
^{93}Y	10.18 h	266.9	7.3	5.127 ± 0.383	5.127 ± 0.383
^{95}Zr	64.02 d	724.3	44.2	6.454 ± 0.454	6.454 ± 0.454
^{97}Zr	16.91 h	743.4	93.0	4.701 ± 0.430	4.701 ± 0.430
^{99}Mo	65.94 h	140.5	89.4	3.033 ± 0.241	3.033 ± 0.241
		739.5	12.13	3.123 ± 0.250	3.123 ± 0.250
^{103}Ru	39.26 d	497.1	90.0	0.533 ± 0.151	0.533 ± 0.151
^{105}Rh	35.36 h	319.1	19.2	0.241 ± 0.028	0.241 ± 0.028
^{112}Ag	3.13 h	617.5	43.0	0.274 ± 0.024	0.274 ± 0.024
^{115}Cd^{g}	53.46 h	527.9	27.45	0.260 ± 0.024	
^{115}Cd^{total}				0.302 ± 0.028*	0.302 ± 0.028*
^{127}Sb	3.85 d	687.0	37.0	0.533 ± 0.052	0.533 ± 0.052
^{128}Sn	59.07 min	482.3	59.0	1.328 ± 0.146	1.412 ± 0.156
^{129}Sb	4.32 h	812.4	43.0	1.706 ± 0.232	1.716 ± 0.233
^{131}I	8.02 d	364.5	81.7	3.052 ± 0.208	3.052 ± 0.208
^{132}Te	3.2 d	228.1	88.0	3.846 ± 0.435	3.877 ± 0.438
^{133}I	20.8 h	529.9	87.0	4.904 ± 0.345	4.909 ± 0.345
^{134}I	52.5 min	847.3	95.9	6.687 ± 0.457	6.700 ± 0.458
		884.09	65.0	6.927 ± 0.487	6.947 ± 0.488
^{135}I	6.57 h	1131.5	22.7	5.262 ± 0.416	5.316 ± 0.421
		1260.4	20.3	5.609 ± 0.706	5.665 ± 0.713
^{139}Ba	83.03 min	165.8	23.7	7.031 ± 0.562	7.031 ± 0.562
^{140}Ba	12.75 d	537.3	35.4	8.240 ± 0.524	8.240 ± 0.524
^{141}Ce	32.5 d	145.4	20.5	6.984 ± 0.743	6.984 ± 0.743
^{142}La	91.1 min	641.3	47.0	6.119 ± 0.317	6.119 ± 0.317
^{143}Ce	33.03 h	293.3	42.8	6.766 ± 0.581	6.766 ± 0.581
^{147}Nd	10.98 d	531.0	13.1	2.351 ± 0.274	2.358 ± 0.275
^{150}Pm	2.68 h	333.97	68.0	0.581 ± 0.019	0.582 ± 0.019

Y_C – Cumulative yields, Y_A – Mass yields, ^{92}Sr – Fission rate monitor.
*The yields of ^{115}Cd^{total} is based on the ratio of ^{115}Cd^{g}/^{115}Cd^{m} = 6 as done in Ref. [50].

and bremsstrahlung induced fission of ^{232}Th, the yields of fission products for A = 133–134, 138–140, 143–144 and their complementary products are higher than the other fission products. The mass numbers of 133–134, 138–140 and 143–144 correspond to the most probable even charge of 52, 54 and 56. Thus the oscillation of fission yields in the interval of five mass units around the mass region of 133–144 is due to the even–odd effect [75]. Since the A/Z ratio of the fission products and fissioning systems are around 2.5, the change of oscillation of mass yields occurs in the interval of five mass units. Besides this, the higher yields of fission products for A = 134–134 and 143–144 can also be explained from the point of view of the standard I and standard II asymmetric fission modes as mentioned by Brossa et al. [76], which arise due to shell effects [77]. Based on standard I asymmetry, the fissioning system is characterized by spheri-

Table 3
Nuclear spectroscopic data and yields of fission products in the 9.35 MeV neutron-induced fission of ^{232}Th.

Nuclide	Half-life	γ-Ray energy (keV)	γ-Ray abundance (%)	Y_C (%)	Y_A (%)
^{85}Kr^{m}	4.48 h	151.2	75.0	3.124 ± 0.182	3.124 ± 0.182
		304.9	14.0	3.181 ± 0.251	3.181 ± 0.251
^{87}Kr	76.3 min	402.6	49.6	6.139 ± 0.489	6.158 ± 0.490
^{88}Kr	2.84 h	196.3	25.9	5.427 ± 0.431	5.516 ± 0.438
^{91}Sr	9.63 h	749.8	23.6	5.906 ± 0.386	5.906 ± 0.386
		1024.3	33.0	6.023 ± 0.482	6.023 ± 0.482
^{92}Sr	2.71 h	1383.9	90.0	5.418 ± 0.377	5.429 ± 0.378
^{93}Y	10.18 h	266.9	7.3	4.925 ± 0.343	4.925 ± 0.343
^{95}Zr	64.02 d	724.3	44.2	6.392 ± 0.447	6.392 ± 0.447
^{97}Zr	16.91 h	743.4	93.0	4.838 ± 0.351	4.843 ± 0.352
^{99}Mo	65.94 h	140.5	89.4	2.890 ± 0.230	2.890 ± 0.230
		739.5	12.13	2.790 ± 0.325	2.790 ± 0.325
^{103}Ru	39.26 d	497.1	90.0	0.668 ± 0.082	0.668 ± 0.082
^{105}Rh	35.36 h	319.1	19.2	0.378 ± 0.061	0.378 ± 0.061
^{112}Ag	3.13 h	617.5	43.0	0.538 ± 0.048	0.539 ± 0.048
^{115}Cd^{g}	53.46 h	527.9	27.45	0.454 ± 0.122	
^{115}Cd^{total}				0.529 ± 0.139*	0.529 ± 0.139*
^{127}Sb	3.85 d	687.0	37.0	0.634 ± 0.056	0.634 ± 0.056
^{128}Sn	59.07 min	482.3	59.0	1.002 ± 0.252	1.066 ± 0.268
^{129}Sb	4.32 h	812.4	43.0	1.666 ± 0.256	1.676 ± 0.258
^{131}I	8.02 d	364.5	81.7	3.207 ± 0.256	3.207 ± 0.256
^{132}Te	3.2 d	228.1	88.0	4.305 ± 0.343	3.340 ± 0.346
^{133}I	20.8 h	529.9	87.0	5.351 ± 0.352	5.356 ± 0.352
^{134}I	52.5 min	847.3	95.9	6.305 ± 0.503	6.318 ± 0.504
		884.09	65.0	6.692 ± 0.647	6.705 ± 0.648
^{135}I	6.57 h	1131.5	22.7	5.650 ± 0.963	5.707 ± 0.973
		1260.4	20.3	5.741 ± 0.755	5.799 ± 0.763
^{139}Ba	83.03 min	165.8	23.7	6.830 ± 0.269	6.830 ± 0.269
^{140}Ba	12.75 d	537.3	35.4	7.473 ± 0.525	7.473 ± 0.525
^{141}Ce	32.5 d	145.4	20.5	6.123 ± 0.369	6.123 ± 0.369
^{142}La	91.1 min	641.3	47.0	5.559 ± 0.469	5.559 ± 0.469
^{143}Ce	33.03 h	293.3	42.8	6.028 ± 0.286	6.028 ± 0.286
^{147}Nd	10.98 d	531.0	13.1	1.996 ± 0.108	2.002 ± 0.109
^{150}Pm	2.68 h	333.97	68.0	0.438 ± 0.017	0.439 ± 0.017

Y_C – Cumulative yields, Y_A – Mass yields, ^{92}Sr – Fission rate monitor.
*The yields of ^{115}Cd^{total} is based on the ratio of ^{115}Cd^{g}/^{115}Cd^{m} = 6 as done in Ref. [50].

cal heavy fragment with mass numbers 133–134 due to the spherical 82n shell and a deformed complementary light mass fragment. Based on standard II asymmetry, the fissioning system is characterized by a deformed heavy-mass fragment near the mass numbers of 143–144 due to a deformed 86–88n shell and slightly deformed light mass fragment. Thus, the higher yields of fission products for $A = 133$–134 and 143–144 are due to the presence of spherical 82n and deformed 86–88n shells, respectively. However, it is **surprising** to see from Fig. 1 and Fig. 2 that the yields of fission products for $A = 133$–134 in ^{232}Th(n, f) reaction are significantly higher than in the ^{232}Th(γ, f) reaction. In order to examine this aspects, the yields of fission products for $A = 133$, 139 and 143 from the present work (Tables 1–4) and literature data in the ^{232}Th(n, f) [26–50] and ^{232}Th(γ, f) [52–62] reactions are plotted in Fig. 3 as a function of excitation energy.

Table 4
Nuclear spectroscopic data and yields of fission products in the 12.53 MeV neutron-induced fission of ^{232}Th.

Nuclide	Half-life	γ-Ray energy (keV)	γ-Ray abundance (%)	Y_C (%)	Y_A (%)
^{85}Kr^{m}	4.48 h	151.2	75.0	3.119 ± 0.250	3.119 ± 0.250
		304.9	14.0	3.210 ± 0.258	3.210 ± 0.258
^{87}Kr	76.3 min	402.6	49.6	5.459 ± 0.171	5.475 ± 0.171
^{88}Kr	2.84 h	196.3	25.9	5.109 ± 0.504	5.192 ± 0.512
^{91}Sr	9.63 h	749.8	23.6	5.513 ± 0.387	5.513 ± 0.387
		1024.3	33.0	5.671 ± 0.954	5.671 ± 0.954
^{92}Sr	2.71 h	1383.9	90.0	5.063 ± 0.328	5.074 ± 0.329
^{93}Y	10.18 h	266.9	7.3	4.651 ± 0.650	4.651 ± 0.650
^{95}Zr	64.02 d	724.3	44.2	5.934 ± 0.583	5.934 ± 0.583
^{97}Zr	16.91 h	743.4	93.0	4.672 ± 0.329	4.677 ± 0.329
^{99}Mo	65.94 h	140.5	89.4	2.902 ± 0.233	2.902 ± 0.233
		739.5	12.13	2.819 ± 0.258	2.819 ± 0.258
^{103}Ru	39.26 d	497.1	90.0	0.858 ± 0.051	0.858 ± 0.051
^{105}Rh	35.36 h	319.1	19.2	0.629 ± 0.054	0.629 ± 0.054
^{112}Ag	3.13 h	617.5	43.0	0.791 ± 0.058	0.792 ± 0.058
^{115}Cd^{g}	53.46 h	527.9	27.45	0.754 ± 0.096	
^{115}Cd^{total}				0.879 ± 0.112*	0.879 ± 0.112*
^{127}Sb	3.85 d	687.0	37.0	0.791 ± 0.062	0.791 ± 0.062
^{128}Sn	59.07 min	482.3	59.0	1.166 ± 0.092	1.239 ± 0.097
^{129}Sb	4.32 h	812.4	43.0	1.707 ± 0.192	1.716 ± 0.193
^{131}I	8.02 d	364.5	81.7	2.986 ± 0.258	2.986 ± 0.258
^{132}Te	3.2 d	228.1	88.0	4.160 ± 0.287	3.189 ± 0.289
^{133}I	20.8 h	529.9	87.0	5.422 ± 0.550	5.427 ± 0.550
^{134}I	52.5 min	847.3	95.9	6.608 ± 0.426	6.622 ± 0.463
		884.09	65.0	6.167 ± 0.520	6.179 ± 0.522
^{135}I	6.57 h	1131.5	22.7	5.676 ± 0.466	5.733 ± 0.471
		1260.4	20.3	5.438 ± 0.401	5.493 ± 0.405
^{139}Ba	83.03 min	165.8	23.7	7.070 ± 0.496	7.070 ± 0.496
^{140}Ba	12.75 d	537.3	35.4	7.237 ± 0.545	7.237 ± 0.545
^{141}Ce	32.5 d	145.4	20.5	6.279 ± 0.658	6.279 ± 0.658
^{142}La	91.1 min	641.3	47.0	5.796 ± 0.404	5.796 ± 0.404
^{143}Ce	33.03 h	293.3	42.8	5.875 ± 0.637	5.875 ± 0.637
^{147}Nd	10.98 d	531.0	13.1	2.074 ± 0.133	2.080 ± 0.134
^{150}Pm	2.68 h	333.97	68.0	0.458 ± 0.042	0.459 ± 0.042

Y_C – Cumulative yields, Y_A – Mass yields, ^{92}Sr – Fission rate monitor.
*The yields of ^{115}Cd^{total} is based on the ratio of ^{115}Cd^{g}/^{115}Cd^{m} = 6 as done in Ref. [50].

From Fig. 3, it can be seen that at all excitation energy, the yields of fission products for $A = 134$ in the ^{232}Th(n, f) reaction is higher than in the ^{232}Th(γ, f) reaction. On the other hand, the yields of fission products are marginally higher for $A = 143$ in the ^{232}Th(γ, f) reaction than in the ^{232}Th(n, f) reaction. For $A = 139$, the yield of fission products are comparable at all excitation energy for both the ^{232}Th(n, f) and ^{232}Th(γ, f) reactions. Besides this, it was observed that in the ^{232}Th(n, f) reaction, the yield of the fission products for $A = 133$–134 and 143–144 are comparable and decreases from 7% at 2 MeV to 5.5 % at 14.8 MeV [26–50]. On the other hand in the ^{232}Th(γ, f) reaction [52–62], the yield of fission product for $A = 133$–134 increases slightly from 4% at 6.44 MeV to 5% at 85 MeV, whereas for $A = 143$–144, it decrease significantly from 8% at 6.44 MeV to 6% at 25–85 MeV. This difference is based on the presence

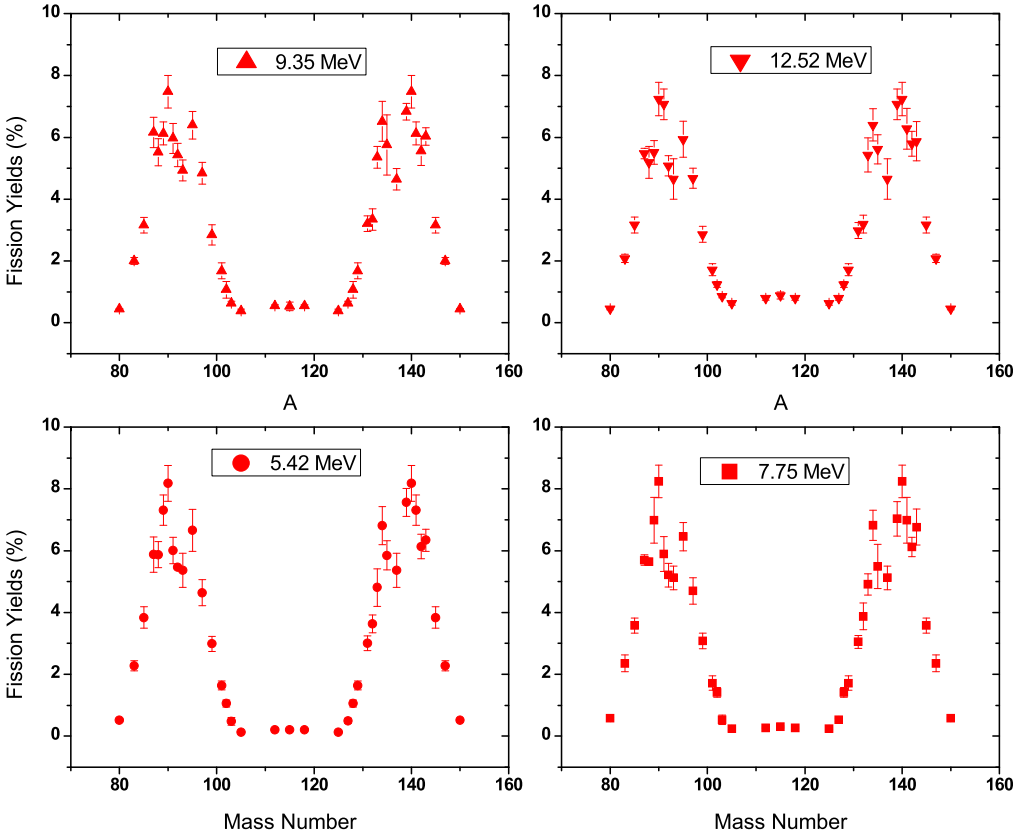

Fig. 1. Plot of mass yields distribution in the quasi-mono-energetic neutron-induced fission of ^{232}Th at 5.42, 7.75, 9.35 and 12.53 MeV.

or absence of shells combination in the complementary pairs as explained in earlier work [78]. The variation of yields data for $A = 133$–134, 139–140 and 143–144 in the $^{232}\mathrm{Th}(n, f)$ and $^{232}\mathrm{Th}(\gamma, f)$ reactions causes variation of the average heavy mass ($\langle A_{\mathrm{H}} \rangle$). In order to examine this, the average heavy mass ($\langle A_{\mathrm{H}} \rangle$) and light mass ($\langle A_{\mathrm{L}} \rangle$) in the $^{232}\mathrm{Th}(n, f)$ reaction from the present work at average neutron energies of 5.42, 7.75, 9.35 and 12.53 MeV as well as at other lower-neutron energies [26–50] were calculated from the mass yields (Y_{A}) of the fission products within the mass ranges of 80–105 and 125–150 by using the following relation:

$$\langle A_{\mathrm{L}} \rangle = \sum (Y_{\mathrm{A}} A_{\mathrm{L}}) \Big/ \sum Y_{\mathrm{A}}, \qquad \langle A_{\mathrm{H}} \rangle = \sum (Y_{\mathrm{A}} A_{\mathrm{H}}) \Big/ \sum Y_{\mathrm{A}} \tag{8}$$

The $\langle A_{\mathrm{L}} \rangle$ and $\langle A_{\mathrm{H}} \rangle$ values obtained from the above relation in the $^{232}\mathrm{Th}(n, f)$ reaction along with their corresponding average excitation energy ($\langle E^* \rangle$) are given in Table 5. The $\langle A_{\mathrm{L}} \rangle$ and $\langle A_{\mathrm{H}} \rangle$ values in the $^{232}\mathrm{Th}(n, f)$ reaction from Table 5 and literature data [52–62] in the $^{232}\mathrm{Th}(\gamma, f)$ reaction are plotted in Fig. 4 as a function of excitation energy. It can be seen from Fig. 4 that at all the excitation energy, the $\langle A_{\mathrm{H}} \rangle$ values are lower in the $^{232}\mathrm{Th}(n, f)$ reaction than in the $^{232}\mathrm{Th}(\gamma, f)$ reaction, whereas the $\langle A_{\mathrm{L}} \rangle$ values are higher in the $^{232}\mathrm{Th}(n, f)$ reaction than in the $^{232}\mathrm{Th}(\gamma, f)$ reaction. This is due to favorable standard I asymmetric mode compared to standard II asymmetric mode of fission in the $^{232}\mathrm{Th}(n, f)$ reaction than in the $^{232}\mathrm{Th}(\gamma, f)$

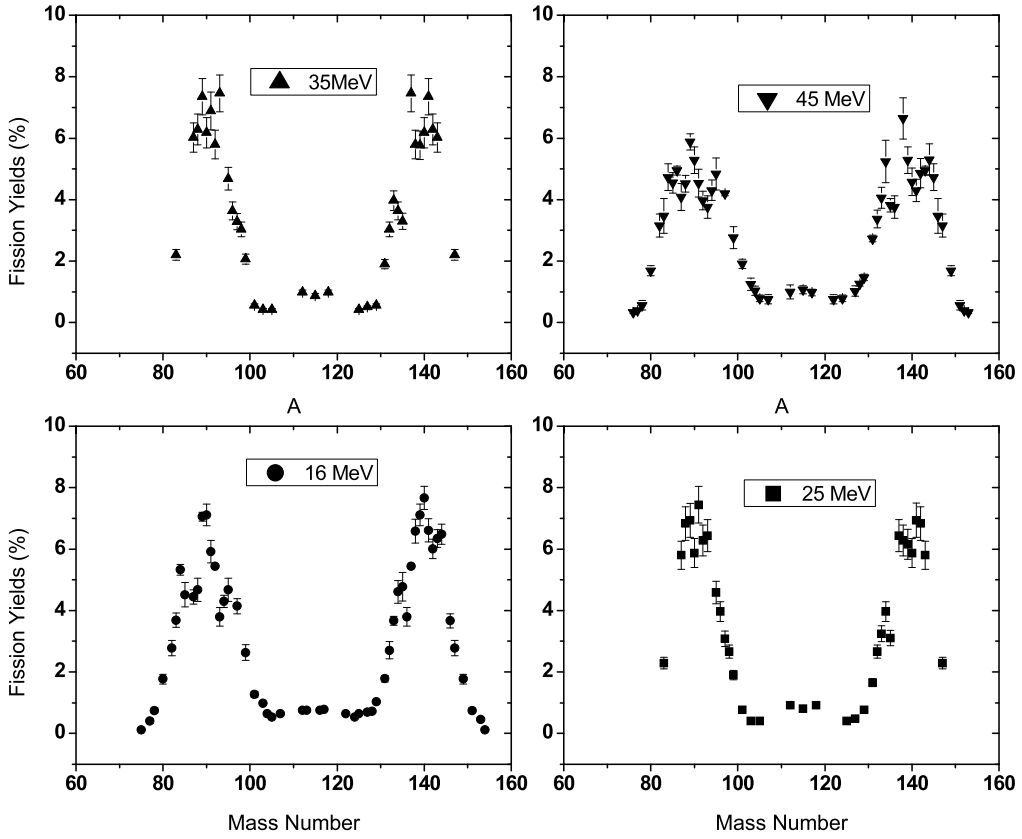

Fig. 2. Plot of mass yields distribution in photon-induced fission of ^{232}Th with bremsstrahlung end-point energies of 16, 25, 35 and 45 MeV.

reaction. Higher $\langle A_L \rangle$ values in ^{232}Th(n, f) reaction than in ^{232}Th(γ, f) reaction are due to the mass conservation based on the standard I and II asymmetric mode of fission. It can be also seen from Fig. 4 that the $\langle A_H \rangle$ values for both ^{232}Th(n, f) and ^{232}Th(γ, f) reactions decrease with the excitation energy, whereas, the $\langle A_L \rangle$ values increase with the excitation energy. However, it is **surprising** to see that the $\langle A_H \rangle$ value in the ^{232}Th(γ, f) reaction within the excitation energy of 10 to 14 MeV are unusually high and then shows a decreasing trend. On the other hand, the $\langle A_L \rangle$ shows the reverse trend to conserved the mass of the fissioning system. The onset of $\langle A_H \rangle$ and $\langle A_L \rangle$ values in the ^{232}Th(n, f) reaction within excitation energy of 10–14 MeV is due to the GDR effect, which is not observed in the ^{232}Th(γ, f) reaction. This is most probably due to the fact that the data in the ^{232}Th(γ, f) reaction are based on bremsstrahlubg spectrum but not from the data of mono-energetic photon. Besides this, the compound nucleus in the ^{232}Th(n, f) reaction has an odd-mass, whereas in the ^{232}Th(γ, f) reaction it is even-mass. This causes slightly higher fission barrier height [79] for the compound nucleus ^{233}Th* than in ^{232}Th*.

The GDR effect within the excitation energy of 10–14 MeV also plays its role to determine the average neutron number, yield of symmetric fission products and thus in the peak-to-valley (P/V) ratio. Thus from the $\langle A_L \rangle$, $\langle A_H \rangle$ and compound nucleus mass ($A_C = 233$), the experimental average numbers of neutrons ($\langle \nu \rangle_{expt}$) were calculated from the following relation:

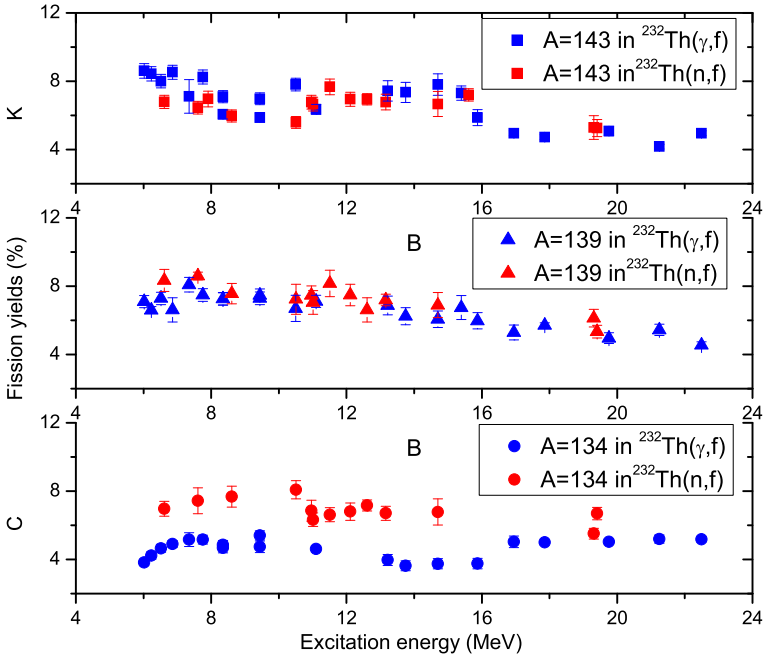

Fig. 3. Plot of yields of fission products (%) as a function of excitation energy for $A = 134$, 139 and 143 in the ^{232}Th(n, f) and ^{232}Th(γ, f) reactions.

$$\langle \nu \rangle_{\text{expt}} = A_{\text{C}} - \left(\langle A_{\text{L}} \rangle + \langle A_{\text{H}} \rangle \right) \tag{9}$$

The $\langle \nu \rangle_{\text{expt}}$ values obtained from the above relation based on the present work and literature data in the ^{232}Th(n, f) reaction [26–50] at different excitation energies are listed in Table 5. The $\langle \nu \rangle_{\text{expt}}$ values for ^{232}Th(n, f) reaction from Table 5 and for ^{232}Th(γ, f) reaction from literature data [52–62] are plotted in Fig. 5 as a function of excitation energy. It can be seen from Fig. 5 that in the neutron and bremsstrahlung induced fission of ^{232}Th, the value of $\langle \nu \rangle_{\text{expt}}$ increases with excitation energy. However, at the same excitation energy, the $\langle \nu \rangle_{\text{expt}}$ value in ^{232}Th(n, f) reaction is higher than in ^{232}Th(γ, f) reaction, which is due to the higher mass in the former than the latter. From Fig. 5, it can also be seen that within the excitation energy of 10–14 MeV, the value of $\langle \nu \rangle_{\text{expt}}$ in ^{232}Th(n, f) reaction is unusually higher than in ^{232}Th(γ, f) reaction, which is due to GDR effect. Thus from the above discussion, it is clear that the increasing trend of $\langle \nu \rangle_{\text{expt}}$ and $\langle A_{\text{L}} \rangle$ as well as decreasing trend of $\langle A_{\text{H}} \rangle$ with excitation energy is not smooth in ^{232}Th(n, f) reaction as in the case of ^{232}Th(γ, f) reaction. This is due to the major GDR effect within excitation energy of 10–14 MeV in the ^{232}Th(n, f) reaction than in the ^{232}Th(γ, f) reaction. Further to examine this aspect, the yields of symmetric products, high yield asymmetric products and the peak-to valley (P/V) ratios from the present work and literature data [26–50] in the ^{232}Th(n, f) reaction are shown in Table 6. The yields of high yield asymmetric products and symmetric products from Table 6 in the ^{232}Th(n, f) reaction and similar data from literature [52–62] in the ^{232}Th(γ, f) reaction are plotted in Fig. 6 as a function of excitation energy.

It can be seen from Fig. 6 that in both the ^{232}Th(n, f) and ^{232}Th(γ, f) reactions, the yields of asymmetric products decrease slightly, whereas the yields of symmetric products increase significantly with excitation energy. It can be also seen from Fig. 6 that in the ^{232}Th(γ, f)

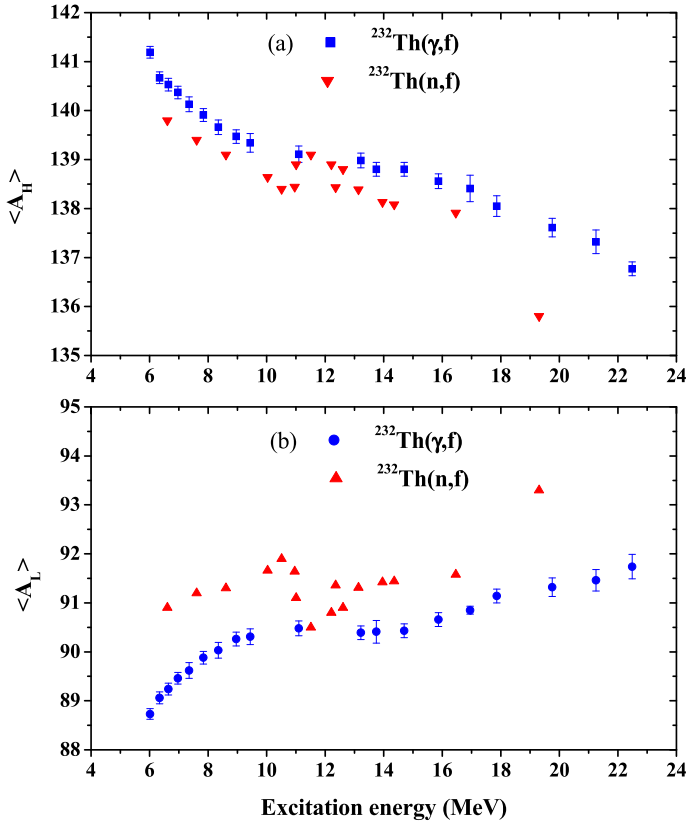

Fig. 4. Plot of average values of heavy mass ($\langle A_{\mathrm{H}}\rangle$) and light mass ($\langle A_{\mathrm{L}}\rangle$) as a function of excitation energy in the ^{232}Th(n, f) and ^{232}Th(γ, f) reactions.

reaction, the yields of symmetric products increase sharply up to the excitation energy of 8 MeV and thereafter increase slowly. This is because the even–odd effect survives up to the excitation 2Δ above the fission barrier. Thus the even–odd effect in the ^{232}Th(γ, f) reaction remain almost constant up to the excitation energy of 8 MeV [80]. In the ^{232}Th(n, f) reaction, the yields of symmetric products increase sharply up to the excitation energy of 10 MeV instead of 8 MeV. This may be due to the higher symmetric fission barrier height [79] in ^{233}Th* due to the odd mass number. Above the excitation energy of 10 MeV, the symmetric products yields slightly decrease up to 14 MeV and then increases. Thus in the ^{232}Th(n, f) reaction, the increase trend of the symmetric products yields with excitation energy is not smooth. On the other hand, in the ^{232}Th(γ, f) reaction, the increase trend of the yields of symmetric products is nearly smooth with excitation energy. The different behavior of symmetric products yields in the ^{232}Th(n, f) reaction compared to the ^{232}Th(γ, f) reaction within excitation energy of 10–14 MeV is due to the GDR effect. Similar effect within the excitation energy of 10–14 MeV was also seen in the proton induced fission of ^{232}Th [81], which supports the present observation. Further, it can be seen from Fig. 6 that within the excitation energy of 6–18 MeV, the yields of symmetric products are higher in the ^{232}Th(γ, f) reaction than in the ^{232}Th(n, f) reaction and thus the peak-to-valley (P/V) ratio is expected to show the reverse trend. So the P/V ratio in ^{232}Th(n, f)

Table 5
Average light mass ($\langle A_L \rangle$), heavy mass ($\langle A_H \rangle$), and average neutron numbers ($\langle \nu \rangle_{expt}$) in the neutron-induced fission of ^{232}Th.

E_n (MeV)	E^* (MeV)	$\langle A_L \rangle$	$\langle A_H \rangle$	$\langle \nu \rangle_{expt}$	Ref.
2.0	6.61	90.9	139.8	2.3	[43]
3.0	7.61	91.2	139.4	2.4	[43]
4.0	8.61	91.3	139.1	2.6	[43]
5.42	10.03	91.66	138.64	2.7	[A]
5.9	10.51	91.9	138.4	2.7	[43]
6.35	10.96	91.64	138.44	2.91	[50]
6.4	11.01	91.1	138.9	3.0	[43]
6.9	11.51	90.5	139.1	3.4	[43]
7.6	12.21	90.8	138.9	3.3	[43]
7.75	12.36	91.36	138.43	3.2	[A]
8.0	12.61	90.9	138.8	3.3	[43]
8.53	13.14	91.31	138.39	3.4	[50]
9.35	13.96	91.42	138.13	3.45	[A]
10.09	14.36	91.44	138.08	3.48	[50]
11.0	15.61	–	–	–	[27]
12.53	17.14	91.58	137.91	3.51	[A]
14.7	19.31	–	–	–	[47]
14.8	19.41	93.3	135.8	3.9	[28]

A – Present work.

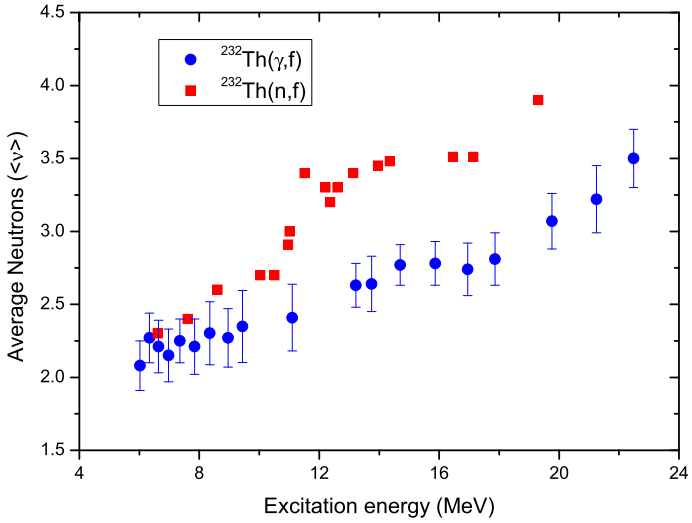

Fig. 5. Plot of average neutron number ($\langle \nu \rangle$) as a function of excitation energy in the ^{232}Th(n, f) and ^{232}Th(γ, f) reactions.

reaction from Table 6 and similar data from literature [52–62] in the ^{232}Th(γ, f) reaction are plotted in Fig. 7 as a function of excitation energy. It can be seen from Fig. 7 that within the excitation energy of 6–18 MeV, the P/V ratio in the ^{232}Th(n, f) reaction is higher than in the ^{232}Th(γ, f) reaction. This is may be due to the odd mass number of the fissioning system ^{233}Th* compared to ^{232}Th*, resulting from slightly higher symmetric fission barrier [79] in the former than latter as mentioned before besides the role of excitation energy. It can be also seen from

Table 6
Yields of asymmetric (Y_a) and symmetric (Y_s) products and P/V ratio in neutron-induced fission of ^{232}Th.

E_n (MeV)	E^* (MeV)	Y_a (%)	Y_s (%)	P/V ratio	Ref.
1.60 ± 0.02	6.21	–	–	218.9 ± 47.7	[42]
1.68 ± 0.02	6.29	–	–	205.1 ± 42.1	[42]
1.72 ± 0.02	6.33	–	–	292.7 ± 73.2	[42]
1.77 ± 0.02	6.38	–	–	241.5 ± 58.8	[42]
1.88 ± 0.02	6.49	–	–	238.2 ± 36.5	[42]
2.00 ± 0.02	6.61	–	–	283.5 ± 64.9	[42]
2.00	6.61	8.950 ± 0.250	0.005 ± 0.001	–	[43]
2.20 ± 0.02	6.81	–	–	212.3 ± 53.9	[42]
2.43 ± 0.02	7.04	–	–	214.5 ± 35.6	[42]
2.96 ± 0.41	7.57	–	–	118.5 ± 17.5	[42]
2.97	7.58	–	–	122.0	[38]
3.00	7.61	8.600 ± 0.230	0.023 ± 0.004	–	[43]
3.00	7.61	7.890 ± 0.094	0.045 ± 0.009	–	[28]
3.10 ± 0.15	7.71	–	–	63.0 ± 11.0	[44]
4.00	8.61	8.010 ± 0.200	0.099 ± 0.015	80.9 ± 12.3	[43]
4.03 ± 0.02	8.64	–	–	71.0	[38]
4.20 ± 0.11	8.81	–	–	27.2 ± 3.1	[42]
4.81 ± 0.02	9.52	–	–	51.0	[38]
5.20 ± 0.25	9.87	–	–	29.0 ± 3.0	[44]
5.30 ± 0.11	9.91	–	–	26.4 ± 2.1	[42]
5.42	10.03	8.177 ± 0.574	0.209 ± 0.038	39.1 ± 7.6	[A]
5.90	10.51	8.080 ± 0.530	0.270 ± 0.040	29.9 ± 4.8	[43]
6.35	10.96	8.358 ± 0.551	0.277 ± 0.028	30.3 ± 4.4	[50]
6.40	11.01	8.410 ± 0.630	0.230 ± 0.040	36.6 ± 6.9	[43]
6.90	11.51	8.700 ± 0.340	0.200 ± 0.030	43.5 ± 6.7	[43]
7.60	12.21	8.380 ± 0.230	0.200 ± 0.030	41.9 ± 6.4	[43]
7.75	12.36	8.240 ± 0.524	0.302 ± 0.028	27.3 ± 3.1	[A]
8.00	12.61	7.870 ± 0.350	0.290 ± 0.030	27.1 ± 3.9	[43]
8.53	13.14	8.299 ± 0.579	0.487 ± 0.097	17.1 ± 3.6	[50]
9.10 ± 0.30	13.71	(8.000 ± 0.500)	0.436 ± 0.014	18.3 ± 1.3	[29]
9.35	13.96	7.473 ± 0.525	0.529 ± 0.139	13.9 ± 1.6	[A]
10.09	14.70	7.579 ± 0.491	0.655 ± 0.123	11.6 ± 2.6	[50]
11.00	15.61	8.100 ± 0.900	0.760 ± 0.015	10.7 ± 1.3	[27]
12.53	17.14	7.237 ± 0.545	0.879 ± 0.112	8.24 ± 1.22	[A]
13.40 ± 0.17	18.01	(8.000 ± 0.500)	1.440 ± 0.020	5.60 ± 0.36	[29]
14.10 ± 0.16	18.71	(7.500 ± 0.500)	1.340 ± 0.020	5.60 ± 0.38	[29]
14.70 ± 0.30	19.31	(7.500 ± 0.500)	1.580 ± 0.050	4.75 ± 0.51	[47]
14.70 ± 0.30	19.31	–	1.400 ± 0.050	5.36 ± 0.41	[47]
14.70 ± 0.30	19.31	–	1.310 ± 0.140	5.73 ± 0.72	[35]
14.70 ± 0.30	19.31	–	1.380 ± 0.120	5.43 ± 0.59	[45]
14.80 ± 0.80	19.41	6.690 ± 0.325	1.720 ± 0.500	3.89 ± 1.15	[28]
14.80 ± 0.80	19.41	–	1.500 ± 0.200	4.46 ± 0.65	[31]
14.80 ± 0.80	19.41	–	1.240 ± 0.200	5.40 ± 0.92	[30]
14.90 ± 0.25	19.51	(6.500 ± 0.500)	1.280 ± 0.040	5.10 ± 0.42	[29]
18.10 ± 0.25	22.71	(6.500 ± 0.500)	1.920 ± 0.100	3.40 ± 0.31	[29]

A – Present work.

Fig. 7 that in both the ^{232}Th(n, f) and the ^{232}Th(γ, f) reactions, the P/V ratio decrease with excitation energy. However, the P/V ratio in ^{232}Th(n, f) reaction decreases up to 10 MeV and then slightly increases up to 14 MeV and thereafter again decrease, which is due to the GDR effect.

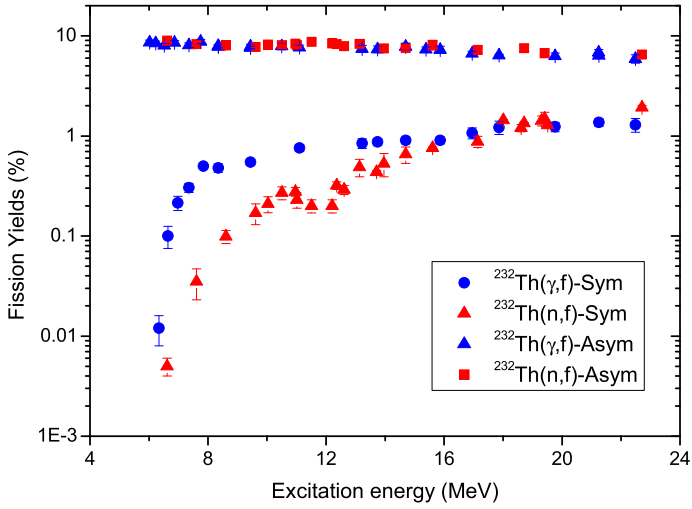

Fig. 6. Plot of symmetric and asymmetric products yields (%) as a function of excitation energy in the ^{232}Th(n, f) and ^{232}Th(γ, f) reactions.

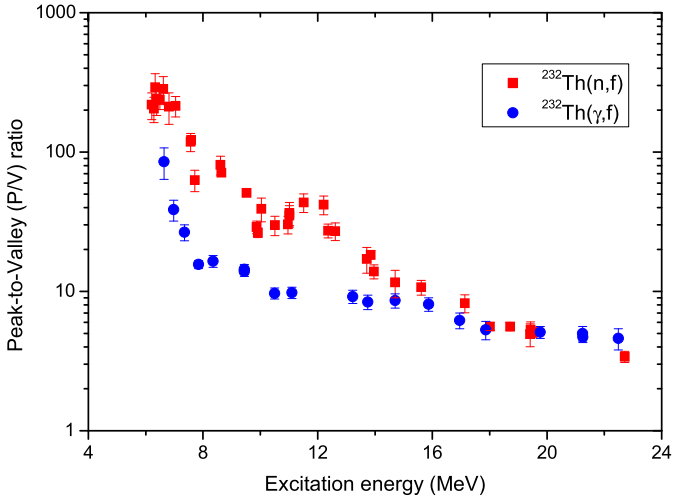

Fig. 7. Plot of peak-to-valley (P/V) ratio as a function of excitation energy in the ^{232}Th(n, f) and ^{232}Th(γ, f) reactions.

5. Conclusions

(i) The cumulative yields of various fission products were determined in the 5.42, 7.75, 9.35 and 12.53 MeV quasi-mono-energetic neutron-induced fission of ^{232}Th by using an off-line γ-ray spectrometric technique. The mass yields were obtained from the cumulative yields of the fission products by using charge distribution corrections and are found to be triple humped similarly to the ^{232}Th(γ, f) reaction.

(ii) The cumulative yields of fission products for $A = 133$–134, $A = 138$–140, and $A = 143$–144 and their complementary products are higher than those of other fission products for

^{232}Th(n, f) and ^{232}Th(γ, f) reactions. This is due to shell closure proximity based on standard I and II asymmetric mode of fission besides the role of even–odd effect.

(iii) In the ^{232}Th(n, f) and ^{232}Th(γ, f) reactions, the $\langle\nu\rangle$ and $\langle A_{\mathrm{L}}\rangle$ values increase and $\langle A_{\mathrm{H}}\rangle$ values decrease with excitation energies. However, within the excitation energy of 10–14 MeV, the increasing trends of $\langle\nu\rangle$ and $\langle A_{\mathrm{L}}\rangle$, and decreasing trend of $\langle A_{\mathrm{H}}\rangle$ with excitation energy are sharper in ^{232}Th(n, f) reaction. This is due to major GDR effect in the ^{232}Th(n, f) reaction than in the ^{232}Th(γ, f) reaction.

(iv) In both the ^{232}Th(n, f) and ^{232}Th(γ, f) reactions, the yields of high yield asymmetric products decrease marginally, whereas for symmetric products increase sharply with excitation energies. However, the increase trend of the symmetric products yields with excitation energy is smooth in the ^{232}Th(γ, f) reaction. On the other hand, in the ^{232}Th(n, f) reaction the yields of symmetric products increase sharply up to the excitation energy of 10 MeV and then decrease up to 14 MeV, which may be due to GDR effect. Above 14 MeV, again it increases with excitation energy.

(v) The P/V ratios in both the ^{232}Th(n, f) and ^{232}Th(γ, f) reactions decrease with excitation energy. However, at all excitation energies, the P/V ratio in the ^{232}Th(n, f) reaction are higher than in the ^{232}Th(γ, f) reaction. This is due to the one mass difference between the two fissioning systems causing difference in symmetric fission barrier between them. The P/V ratio within the excitation energy of 10–14 MeV also shows the GDR effect in the ^{232}Th(n, f) reaction.

References

[1] Fast Reactors and Accelerator Driven Systems Knowledge Base, IAEA-TECDOC-1319: Thorium fuel utilization: options and trends, Nov. 2002.
[2] L. Mathieu, et al., Proportion for a very simple thorium molten salt reactor, in: Proceedings of the Global International Conference, Tsukuba, Japan, 2005, Paper No. 428.
[3] A. Nuttin, D. Heuer, A. Billebaud, R. Brissot, C. Le Brun, E. Liatard, J.M. Loiseaux, L. Mathieu, O. Meplan, E. Merle-Lucotte, H. Nifenecker, F. Perdu, S. David, Progr. Nucl. Energy 46 (2005) 77.
[4] T.R. Allen, D.C. Crawford, Sci. Technol. Nucl. Install. 2007 (2007) 97486.
[5] P.E. MacDonald, N. Todreas, Annual project status report 2000, MIT-ANP-PR-071, INEFL/EXT-2009-00994.
[6] R.K. Sinha, A. Kakodkar, Nucl. Eng. Des. 236 (2006) 683.
[7] S. Ganesan, Creation of Indian experimental benchmarks for thorium fuel cycle, IAEA Coordinated research project on "Evaluated Data for Thorium–Uranium Fuel Cycle", Third Research Co-ordination Meeting, 30 January to 2 February 2006, Vienna, Austria, INDC (NDS)-0494 (2006).
[8] F. Carminati, R. Klapisch, J.P. Revol, Ch. Roche, J.A. Rubia, C. Rubia, An energy amplifier for cleaner and inexhaustible nuclear energy production Driven by particle beam accelerator, CERN/AT/93-49 (ET) 1993.
[9] C.D. Bowman, Proc. of Int. Conf. on Accelerator-Driven Transmutation Technologies and Applications, Las Vegas, NV, USA, AIP Conf. Proc., vol. 346, 1994.
[10] E.D. Arthur, S.A. Schriber, A. Rodriguez (Eds.), The International Conference on Accelerator-Driven Transmutation Technologies and Applications, Las Vegas, Nevada, USA, 1994, AIP Conf. Proc., vol. 346, 1995.
[11] C. Rubia, J.A. Rubio, S. Buono, F. Carminati, N. Fietier, J. Galvez, C. Geles, Y. Kadi, R. Klapisch, P. Mandrilion, J.P. Revol, Ch. Roche, CERN/AT/95-44 (ET) 1995, CERN/AT/95-53 (ET) 1995, CERN/LHC/96-01 (LET) 1996, CERN/LHC/97-01 (EET) 1997.
[12] Accelerator driven systems: energy generation and transmutation of nuclear waste, Status report, IAEA, Vienna, IAEA-TECDO-985, 1997.
[13] C.D. Bowman, Annu. Rev. Nucl. Part. Sci. 48 (1998) 505.
[14] S. Boyer, D. Dassie, J.N. Wilson, M. Aiche, G. Barreau, S. Czajkowski, C. Grosjean, A. Guiral, B. Haas, B. Osmanov, G. Aerts, E. Berthoumieux, P. Gunsing, Ch. Theisen, N. Thiolliere, L. Perrot, Nucl. Phys. A 775 (2006) 175.
[15] K. Oyamatsu, H. Takeuchi, M. Sagisaka, J. Katakura, J. Nucl. Sci. Technol. 38 (2001) 477.
[16] C. Wagemans, The Nuclear Fission Process, CRC, London, 1990.

[17] R. Vandenbosch, J.R. Huizenga, Nuclear Fission, Academic, New York, 1973.
[18] A.C. Wahl, At. Data Nucl. Data Tables 39 (1988) 1.
[19] T.R. England, B.F. Rider, Evaluation and compilation of fission product yields, ENDF-349, LA-UR-94-3106, 1993; B.F. Rider, Compilation of fission products yields, NEDO, 12154 3c ENDF-327, Valecicecitos Nuclear Centre, 1981.
[20] J.R. England, B.F. Rider, ENDF/B-6 FPY: the ENDF/B-6 fission-product yield sublibraries, IAEA-NDS-106, 1995; J.R. England, B.F. Rider, Evaluation and compilation of fission products yields, ENDF/BVI, 1989, 1992.
[21] M. James, R. Mills, Neutron fission products yields, UKFY2 1991, JEF-2.2 1993.
[22] M.A. Kellett, O. Bersillon, R.W. Mills, The JEFF-3.1/-3.1.1 radioactive decay data and fission yields sub-libraries, JEFF report 20, NEA No. 6287, 2009.
[23] IAEA-EXFOR database, at http://www-nds.iaea.org/exfor.
[24] R.H. Iyer, C.K. Mathews, N. Ravindran, K. Rengan, D.V. Singh, M.V. Ramaniah, H.D. Sharma, J. Inorg. Nucl. Chem. 25 (1963) 465.
[25] H.N. Erten, A. Grutter, E. Rossler, H.R. von Gunten, Nucl. Sci. Eng. 79 (1981) 167.
[26] A. Turkevich, J.B. Nidday, Phys. Rev. 84 (1951) 52.
[27] A. Turkevisch, J.B. Nidday, A. Tompkins, Phys. Rev. 89 (1953) 552.
[28] K.M. Broom, Phys. Rev. 133 (1964) B874.
[29] G.P. Ford, R.B. Leachman, Phys. Rev. B 137 (1965) 826.
[30] R. Ganapathy, P.K. Kuroda, J. Inorg. Nucl. Chem. 28 (1966) 2071.
[31] Tin Mo, M.N. Rao, J. Inorg. Nucl. Chem. 30 (1968) 345.
[32] M. Thin, M.N. Rao, P.K. Kurdo, J. Inorg. Nucl. Chem. 30 (1968) 1145.
[33] A.I. Sagachev, V.G. Vorobeieva, B.D. Kuzminov, V.B. Mikhaylov, Z. Tarsko, Sov. J. Nucl. Phys. 7 (1968) 475.
[34] S.J. Lyle, J. Sellears, Radiochim. Acta 12 (1969) 43.
[35] L.H. Gevaert, R.E. Jervis, H.D. Sharma, Can. J. Chem. 48 (1970) 641.
[36] J. Blachot, L.C. Carraz, P. Cavallini, E. Monnand, F. Schusslor, J. Radioanal. Nucl. Chem. 7 (1971) 309.
[37] D.L. Swindle, D.T. Moore, J.N. Beck, P.K. Kuroda, J. Inorg. Nucl. Chem. 33 (1971) 3643.
[38] W. Holubarsch, L. Pfeiffer, F. Gonnenwein, Nucl. Phys. A 171 (1971) 631.
[39] S.A. Rao, Phys. Rev. 5 (1972) 171.
[40] J.P. Bocquet, R. Brissot, J. Crancon, A. Moussa, Nucl. Phys. A 189 (1972) 556.
[41] S.M. Dubroviva, V.I. Nogorodtseva, L.N. Morozov, V.A. Pchevin, L.V. Chistyakov, V.A. Schigin, V.M. Shubko, Yad. Fiz. 17 (1973) 1470.
[42] J. Trochon, H.A. Yehia, F. Brisard, Y. Pranal, Nucl. Phys. A 318 (1979) 63.
[43] L.E. Glendenin, J.E. Gindler, I. Ahmad, D.J. Henderson, J.W. Meadows, Phys. Rev. C 22 (1980) 152.
[44] S.T. Lam, L.L. Yu, H.W. Fielding, W.K. Dawson, G.C. Neilson, Phys. Rev. C 28 (1983) 1212.
[45] A.E. Richoortson, H.L. Wright, J.L. Meason, J.R. Smith, Nucl. Sci. Eng. 94 (1986) 413.
[46] Li. Wenxin, S. Tongyu, S. Xiuhua, Fu Ming, D. Tianrong, High Energy Phys. Nucl. Phys. 11 (1887) 376 (Chinese).
[47] S. Tongyu, Li Wenxin, D. Tianrong, Fu Ming, High Energy Phys. Nucl. Phys. 12 (1888) 221 (Chinese).
[48] V.D. Simutkin, I.V. Ryzhov, G.A. Tutin, L.A. Vaishnene, J. Blongren, S. Pomp, M. Oesterlung, P. Andersson, R. Bevilacqua, J.P. Menlders, R. Prieels, AIP Conf. Proc. 1175 (2010) 393.
[49] P.M. Prajapati, H. Naik, S. Mukherjee, S.V. Suryanarayana, B.S. Shivashankar, R. Crasta, V.K. Mulik, K.C. Jagadeesan, S.V. Thakre, A. Goswami, Nucl. Sci. Eng. 176 (2014) 1.
[50] H. Naik, Rita Crasta, S.V. Suryanarayana, P.M. Prajapati, V.K. Mulik, B.S. Shivasankar, K.C. Jagadeesan, S.V. Thakare, S.C. Sharma, A. Goswami, Eur. Phys. J. A 50 (2014) 144.
[51] I.V. Ryzhov, S.G. Yavshits, G.A. Tutin, N.V. Kovalev, A.V. Saulski, N.A. Kudryashev, A.V. Saulski, N.A. Kudryashev, M.S. Onegin, L.A. Vaishnene, Yu.A. Gavrikov, O.T. Grudzevich, V.D. Simutkin, S. Pomp, J. Blomgren, M. Osterlund, P. Andersson, R. Bevilacqua, J. Meulders, R. Prieels, Phys. Rev. C 85 (2011) 054603.
[52] D.M. Hiller, D.S. Martin Jr., Phys. Rev. 90 (1953) 581.
[53] L.H. Gevaert, R.E. Jervis, S.C. Subbarao, H.D. Sharma, Can. J. Chem. 48 (1970) 652.
[54] B. Schrøder, G. Nydahl, B. Forkman, Nucl. Phys. A 143 (1970) 449.
[55] A. Chattopadhyay, K.A. Dost, I. Krajbich, H.D. Sharma, J. Inorg. Nucl. Chem. 35 (1973) 2621.
[56] J.C. Hogan, A.E. Richardson, J.L. Meason, H.L. Wright, Phys. Rev. C 16 (1977) 2296.
[57] W. Gunther, K. Huber, U. Kneissl, H. Krieger, H.J. Maier, Z. Phys. A 295 (1980) 333.
[58] M. Piessens, E. Jacobs, S. Pomm´e, D. De Frenne, Nucl. Phys. A 556 (1993) 88.
[59] H. Naik, T.N. Nathaniel, A. Goswami, G.N. Kim, M.W. Lee, S.V. Suryanarayana, S. Ganesan, E.A. Kim, M.-H. Cho, K.L. Ramakumar, Phys. Rev. C 85 (2012) 024623.
[60] H. Naik, A. Goswami, G.N. Kim, M.W. Lee, K.S. Kim, S.V. Suryanarayana, E.A. Kim, M.-H. Cho, Phys. Rev. C 86 (2012) 054607.

[61] H. Naik, V.T. Nimje, D. Raj, S.V. Suryanarayana, A. Goswami, S. Singh, S.N. Acharya, K.C. Mttal, S. Ganesan, P. Chandrachoodan, V.K. Manchanda, V. Venugopal, S. Banarjee, Nucl. Phys. A 853 (2011) 1.
[62] H. Naik, G.N. Kim, R. Schwengner, K. Kim, R. John, R. Massarczyk, A. Junghans, A. Wagner, A. Goswami, Eur. Phys. J. A 51 (2015) 150.
[63] K.-H. Schmidt, S. Steinhäuser, C. Böckstiegel, A. Grewe, A. Heinz, A.R. Junghans, J. Benlliure, H.-G. Clerc, M. de Jong, J. Müller, M. Pfützner, B. Voss, Nucl. Phys. A 665 (2000) 221.
[64] S. Steinhäuser, J. Benlliure, C. Böckstiegel, H.-G. Clerc, A. Heinz, A. Grewe, M. de Jong, A.R. Junghans, J. Müller, M. Pfützner, K.-H. Schmidt, Nucl. Phys. A 634 (1998) 89.
[65] J. Benlliure, A.R. Junghans, K.-H. Schmidt, Eur. Phys. J. A 13 (2002) 93.
[66] H. Umezawa, S. Baba, H. Baba, Nucl. Phys. A 160 (1971) 65.
[67] J.F. Ziegler, J.P. Biersack, U. Littmark, The Stopping and Range of Ions in Solids, Pergamon, New York, 1999; J.F. Ziegler, J.P. Biersack, U. Littmark, SRIM 2003 code, www.SRIM.org/SRIM2003.html.
[68] H. Liskien, A. Paulsen, At. Data Nucl. Data Tables 15 (1975) 57.
[69] J.W. Meadows, D.L. Smith, Neutrons from proton bombardment of natural lithium, Argonne National Laboratory report ANL-7983, 1972.
[70] C.H. Poppe, J.D. Anderson, J.C. Davis, S.M. Grimes, C. Wong, Phys. Rev. C 14 (1976) 438.
[71] E. Browne, R.B. Firestone, in: V.S. Shirley (Ed.), Table of Radioactive Isotopes, Wiley, New York, 1986; R.B. Firestone, L.P. Ekstrom, in: Table of Radioactive Isotopes, 2004, Version 2.1.
[72] J. Blachot, C. Fiche, Ann. Phys. Suppl. 6 (1981) 3.
[73] N. Sugarman, A. Turkevich, in: C.D. Coryell, N. Sugarman (Eds.), Radiochemical Studies: The Fission Product, vol. 3, McGraw-Hill, New York, 1951, p. 1396.
[74] M. Strecker, R. Wein, P. Plischke, W. Scobel, Phys. Rev. C 41 (1990) 2172.
[75] H. Naik, R.J. Singh, R.H. Iyer, Eur. Phys. J. A 16 (2003) 495.
[76] U. Brossa, S. Grossmann, A. Muller, Phys. Rep. 197 (1990) 167.
[77] B.D. Wilkins, E.P. Steinberg, R.R. Chasman, Phys. Rev. C 14 (1976) 1832.
[78] H. Naik, V.K. Mulik, P.M. Prajapati, B.S. Shivasankar, S.V. Suryanarayana, K.C. Jagadeesan, S.V. Thakare, S.C. Sharma, A. Goswami, Nucl. Phys. A 913 (2013) 185.
[79] S. Bjornholm, J.E. Lynn, Rev. Mod. Phys. 52 (1980) 725.
[80] K. Persyn, E. Jacobs, S. Pomme, D. De Frenne, K. Govaert, M.L. Yoneama, Nucl. Phys. A 620 (1997) 171.
[81] H. Kudo, H. Muramatsu, H. Nakahara, K. Miyano, I. Kohno, Phys. Rev. C 25 (1982) 3011.